Paper pa02-061
Submitted to the 28th International Conference on High Energy Physics
ICHEP'96, Warsaw, Poland, July 1996

A Measurement and QCD Analysis of the Diffractive Structure Function $F_2^{D(3)}$

H1 Collaboration

Abstract

A new analysis of diffractive deep-inelastic ep scattering at HERA is presented using data taken in 1994 with the H1 detector corresponding to an integrated luminosity of $\sim 2\,\mathrm{pb}^{-1}$. The cross section is measured in terms of a diffractive structure function $F_2^{D(3)}(\beta, Q^2, x_{I\!P})$ over the kinematic range $2.5 < Q^2 < 65$ GeV$^2/c^2$, $0.01 < \beta < 0.9$ and $0.0001 < x_{I\!P} < 0.05$. The dependence of $F_2^{D(3)}$ on $x_{I\!P}$ is found not to depend on Q^2 but to depend on β, demonstrating that the factorisation of the $\gamma^* p$ cross section into a universal diffractive flux (depending only on $x_{I\!P}$) and a structure function (depending only on β and Q^2) is not tenable. These deviations from factorisation are demonstrated to be consistent with an interpretation in which two individually factorisable components contribute to $F_2^{D(3)}$. These two components may be identified with pomeron ($I\!P$) and meson contributions $\propto x_{I\!P}^{-n_{I\!P}}, x_{I\!P}^{-n_M}$ where $n_{I\!P} = 1.29 \pm 0.03(\mathrm{stat}) \pm 0.07(\mathrm{syst})$ and $n_M = 0.3 \pm 0.3(\mathrm{stat}) \pm 0.6(\mathrm{syst})$. The Q^2 and β dependences of $F_2^{D(3)}$ are examined in the form of $\tilde{F}_2^D(\beta, Q^2)$ after integrating over the dependence on $x_{I\!P}$. For different β, violations of scale invariance are observed in the form of rising dependences of $\tilde{F}_2^D$ on $\log Q^2$ which persist to high values of β, and which are consistent with a substantial gluon component in diffractive exchange. When confronted with the DGLAP evolution equations in perturbative QCD, the data yield first estimates of the partonic content of the diffractive exchange in which gluons carry about 80% of the momentum at $Q^2 \sim Q_0^2 = 2.5\,\mathrm{GeV}^2/\mathrm{c}^2$ and are concentrated near $x_{g/I\!P} = 1$.

1 Introduction

The data taken in 1992 at HERA led to the first observation of deep–inelastic scattering (DIS) events with an interval in rapidity around the proton remnant direction devoid of hadron production - a "rapidity gap" [1, 2]. Using the data taken in 1993, first measurements were made of the contribution of such events to the DIS cross section, quantified in terms of a structure function $F_2^{D(3)}$ [3, 4]. These measurements demonstrated that the rapidity gap events could be attributed to a virtual photon (γ^*)–proton (p) process which is dominantly diffractive. No substantial Q^2 dependence was observed, thus indicating that the sub–structure of diffractive exchange was of a point–like, presumably partonic, nature. First indications for a large gluonic contribution to this partonic sub–structure at high Q^2 were obtained [5, 6, 7]. Considerably more precise 1994 preliminary H1 results on the diffractive structure function are presented here [8].

2 Cross Section for Diffractive Deep-Inelastic Scattering

In order to measure an experimentally well defined cross-section for diffractive deep–inelastic scattering the measurement is defined in terms of the diagram shown in figure 1. The hadronic final state in any event may be decomposed into two systems, X and Y, that are separated by the largest gap in the true rapidity distribution of hadrons in the $\gamma^\star p$ centre of momentum frame. A cross-section is then measured at different values of the invariant masses, M_X and M_Y, of the two systems, interpretable as 'diffractive' when both masses are small by comparison with the centre of mass energy. Under such circumstances, a large rapidity gap must always occur from kinematic considerations alone.

Defining $Q^2 = -q^2$ and $W^2 = (q+P)^2$ in the usual way, where q and P denote the 4-vectors of the virtual photon and the proton respectively, further kinematic variables are defined as

$$t = (P-Y)^2 \qquad x_{I\!P} = \frac{Q^2 + M_X^2}{Q^2 + W^2} \qquad \beta = \frac{Q^2}{Q^2 + M_X^2}.$$

The experimental selection of events is based on the presence of a rapidity gap spanning at least the laboratory range, $3.4 < \eta < 7.5$ [1], inferred from the absence of activity in the Proton Remnant Tagger, Forward Muon Detector, Plug Calorimeter and the more forward part of the Liquid Argon Calorimeter [9]. The system, X, is then taken to be composed of all particles produced backward of the gap. The Lorentz boost in the proton direction of the $\gamma^\star p$ centre of momentum frame allows the mass, M_X to be well reconstructed from the observed tracks and calorimeter deposits in the central and backward regions of the detector.

The lower limit of 7.5 on the rapidity reached by particles in the leading baryonic system, Y, restricts its mass to $M_Y < 1.6$ GeV. This system is not directly observed, though by requiring $x_{I\!P} < 0.05$, we ensure that Y carries in excess of 95% of the incident

[1] The H1 coordinate system is defined such that positive rapidity corresponds to the proton direction.

proton momentum, and the fact that no decay product is observed in the forward detectors implies that the squared momentum transfer [2], $|t| < 1$ GeV^2. Any isospin-exchanging process is likely to be suppressed in this kinematic region, and the system, Y, may be interpreted as a single proton or as a system of particles ($N^\star$, $p\pi\pi$ etc.) with isospin $\frac{1}{2}$. Experimental evidence supporting this is presented in a first measurement of forward neutron production in this event sample[10]. Models of proton dissociation [11, 12, 13] imply that the correction from the measured cross-section ($M_Y < 1.6$ GeV) to one in which the proton vertex is truly elastic is at the level of 5%.

3 Experimental Method

The data presented here were obtained by H1 in 1994, at a time when HERA was colliding 27.5 GeV positrons with protons at 820 GeV. The results shown are based on an integrated luminosity of 2 pb^{-1} with the interaction point in its usual position relative to H1. A further 0.06 pb^{-1} of data taken with the interaction point shifted by 70 cm in the forward (proton) direction are also used, enabling measurements at lower values of Q^2 than would otherwise be possible. Compared to our previous measurement [3], this represents a ten-fold increase in statistics, and the present measurement covers a significantly larger kinematic range.

Deep-inelastic scattering events were triggered by an energy cluster in the backward electromagnetic calorimeter (BEMC), full efficiency being reached for electrons with energy above 8 GeV [9]. A fiducial volume cut on the BEMC cluster and the requirement that it be associated with a charged particle track in the proportional and drift chambers of H1 reduce photoproduction and beam gas backgrounds to negligible levels. To ensure the definition of an event vertex, at least one reconstructed track pointing to the interaction region is required. Diffractive events are selected by requiring no activity above noise in any of the forward detectors and the pseudorapidity of the most forward cluster in the main calorimeter with energy above 400 MeV $\eta_{\max} < 3.4$.

The final state X is reconstructed using a method that combines tracking and calorimeter information in order to optimise the resolution of the hadronic four-vector. The invariant mass M_X is reconstructed solely from the hadronic four-vector, and the requirement that $\eta_{\max} < 3.4$ ensures that the system X is well contained in the calorimeter such that the invariant mass M_X is accurately reconstructed. The deep-inelastic scattering variables x, y and Q^2 are reconstructed with the Σ method [14], which uses information from both X and the scattered electron. This method not only allows good resolution over the entire accessible kinematic range but also substantially reduces radiative corrections to $\sim 3\%$ or below [15].

[2]Note that the range in t is smaller than that in our earlier publication [3] because of the inclusion of the proton remnant tagger, which is sensitive to energy flow at larger rapidity than the other forward detectors.

4 Modelling Deep-Inelastic Processes

The RAPGAP generator [16] is used to model the high mass region ($M_X \gtrsim 1.2$ GeV) of diffractive production. This is a perturbative model based upon diffractive hard scattering in $e^{\pm}$–$I\!P$ collisions for which a partonic substructure is assigned to the $I\!P$. In addition to the leading $\mathcal{O}(\alpha)$ quark parton model diagram ($eq \rightarrow eq$), boson–gluon fusion ($eg \rightarrow eq\bar{q}$) and QCD–compton ($eq \rightarrow eqg$) processes are generated according to the order $\mathcal{O}(\alpha\alpha_s)$ matrix elements. Parton number density functions for the pomeron are from a leading order DGLAP [17] QCD analysis of the measured structure function [8] (see section 7). Fragmentation is provided either by the colour dipole model as implemented in ARIADNE [18] or parton showers as implemented in LEPTO [19]. QED radiative processes are included via an interface to the program HERACLES [20].

The low mass region ($M_X < 1.2$ GeV) is modelled with DIFFVM [11], which produces the vector meson series ρ^0, ω and ϕ. The magnitude, and the Q^2 and W dependences are set to be near to the values as measured [21].

Non-diffraction i.e. the region of high M_Y and/or high M_X is modelled with a mixture of RAPGAPπ exchange and DJANGO [22]. RAPGAP π describes the process $ep \rightarrow enX$, in which the virtual photon undergoes a hard scattering with a virtual pion. A standard pion flux is used ($\alpha(0) = 0$, $\alpha' = 1$) so that the events are predominately produced at high $x_{I\!P}$. DJANGO is a standard non-diffractive generator with a colour string between the proton remnant and the current fragmentation region. Since DJANGO does not reproduce the observed diffractive signal, events with $x_{I\!P} < 0.1$ and $M_X < 5$ GeV were not used for corrections or comparisons.

The fraction of events from each process was chosen in order to best describe the distributions of η_{max}, $x_{I\!P}$ and M_X for the DIS sample both with and without a diffractive selection (see figure 2). The fractions chosen were:

$$f_{RAPGAP I\!P} : f_{RAPGAP\pi} : f_{DIFFVM} : f_{DJANGO} = 0.17 : 0.46 : 0.004 : 0.37$$

It is important to stress that this mixture is no more than a model, which is used for acceptance corrections and which is chosen only because it provides the best overall description of the properties of the data most relevant for the accurate extraction of the cross section described in the following section. It was checked that the final results of the measurement of $F_2^{D(3)}(\beta, Q^2, x_{I\!P})$ did not change within errors by using either DJANGO alone or RAPGAP π alone to model the high $x_{I\!P}$ region. A preliminary analysis of data taken with the H1 leading neutron calorimeter, in which the contribution of charge exchange to both the inclusive and diffractive DIS samples is estimated, is presented elsewhere [10].

5 Evaluation of the Diffractive Structure Function

After all cuts, the data are used to measure a cross-section for the process, $ep \rightarrow e'XY$, differential in $x_{I\!P}$, β and Q^2, in the kinematic range $2.5 < Q^2 < 65$ GeV^2, $0.01 < \beta < 0.9$ and $0.0001 < x_{I\!P} < 0.05$, integrated over the region $M_Y < 1.6$ GeV and $|t| < 1$ GeV^2.

Following the procedure proposed by Ingelman and Schlein in [23], the results are presented in terms of a diffractive structure function $F_2^{D(3)}(\beta, Q^2, x_{I\!P})$ which is related to the differential $ep \to e'XY$ cross section by

$$\frac{\mathrm{d}^3\sigma^D_{ep\to eXY}}{\mathrm{d}x_{I\!P}\,\mathrm{d}\beta\,\mathrm{d}Q^2} = \frac{4\pi\alpha^2}{\beta Q^4}(1-y+\frac{y^2}{2})F_2^{D(3)}(\beta, Q^2, x_{I\!P}).$$

The Monte Carlo models are used to correct bin by bin for losses, smearing and backgrounds. Non–diffractive background in the sample is only subtracted if an event is generated outside the measured kinematic region (i.e. with either $x_{I\!P} > 0.05$ or $M_Y > 1.6$ GeV), and due to resolution effects or to undetected particles is reconstructed within the kinematic region of study. For all the bins selected it is required that the smeared acceptance is above 0.3, the purity (i.e. ratio of number of events both generated and reconstructed in a bin to the number reconstructed in the bin) is greater than 0.2 and the background fraction from unmeasured kinematic regions ($x_{I\!P} > 0.1$ and/or $M_Y > 5$ GeV) is less than 0.2. In order to check the stability of the results the measurement was repeated by widely varying the analysis techniques. Figure 3 shows that there is very little change in the final results for a variety of reconstruction techniques or different gap requirements — indeed, even if no rapidity gap is required very similar results are obtained, well within the quoted systematic uncertainty.

6 Non-factorisation of the Diffractive Structure Function

The quantity, $x_{I\!P} \cdot F_2^{D(3)}(\beta, Q^2, x_{I\!P})$ is shown as a function of $x_{I\!P}$ in figure 4 for different values of β and Q^2. In a Regge interpretation [24], in which the $x_{I\!P}$ dependence is assumed to describe a pomeron flux associated with the proton, one expects a behaviour of the form $F_2^{D(3)} \propto \frac{1}{x_{I\!P}^n}$ with $n = 2\alpha(t)-1$, where $\alpha(t) = \alpha(0)+\alpha' t$ is the effective pomeron trajectory. In practice, the finite values of t at which the measurement takes place are expected to reduce n relative to $2\alpha(0) - 1$ by a few percent. Figure 5a shows the results of fitting the data to the same polynomial dependence $\frac{1}{x_{I\!P}^n}$ where n is allowed to vary with β but not with Q^2 ($\chi^2/ndf = 161/152$). The improved precision and enhanced kinematic range clearly reveals deviations from the universal factorisation observed in [3]. A fit in which n is independent of both β and Q^2 is inconsistent with the data ($\chi^2/ndf = 267/158$). In figure 5b the value of n is allowed to vary with Q^2 but not β. There is no evidence for any dependence of n on $\ln Q^2$, and the resulting β averaged value of n is entirely consistent with our previous measurement [3].

The value of n decreases significantly with β for $\beta \lesssim 0.3$, demonstrating that the factorisation of $F_2^{D(3)}$ into terms depending on β and Q^2 and an $x_{I\!P}$ dependence describing a universal diffractive flux associated with the proton is not valid in the full measured kinematic range. A purely phenomenological fit in which the value of n has no dependence on Q^2 but varies quadratically with β is superimposed in both figure 4 and figure 5. The value of n at $\beta \gtrsim 0.3$ is observed to be slightly larger than that expected for the effective pomeron trajectory from Regge and other theoretical treatments that are based on the kinematic dependences of total, elastic and inelastic diffractive hadron-hadron cross-sections [25, 26, 27, 28]. The measurements of n in [4] and in [30] are consistent with this measurement and its predecessor [3]. The measurement of n in [31], where the cross-section is defined differently, is inconsistent.

There are a number of possible explanations for the decrease in n for $\beta \lesssim 0.2$ to values below unity. One possibility is that there is a small contribution from the exchange of meson trajectories such as the $f_2^0(1270)$, for which one would expect $n \sim 0$, and which may have a much softer β dependence than that of the leading vacuum trajectory. Figure 6 shows a fit to the data in which both a pomeron component $F_2^{I\!P}(\beta,Q^2)\cdot x_{I\!P}^{-n_{I\!P}}$ and meson component $C_M \cdot F_2^M(\beta,Q^2)\cdot x_{I\!P}^{-n_M}$ contribute to $F_2^{D(3)}$. The structure function $F_2^M(\beta,Q^2)$ is taken from a GRV parameterisation of the pion [32]. The overall normalisation of the meson component C_M, the pomeron structure function $F_2^{I\!P}(\beta,Q^2)$, $n_{I\!P}$ and n_M are free parameters in the fit to the data. This procedure yields an equally good description of the data as the phenomenological fit $n = n(\beta)$ described above ($\chi^2/ndf = 165/156$).

No measurements of the structure function of the $f_2^0(1270)$ exist, and so the systematic dependencies of the parameters obtained from the fit on the assumed functional form of the meson component were investigated by adopting a range of function forms for the meson structure function varying between $F_2^M(\beta,Q^2) \propto (1-\beta)^{0.5}$ and $(1-\beta)^4$. The influence of any possible interference between the two components was studied by introducing a relative phase angle varied between 0 and 180^o. The resulting values of $n_{I\!P}$ and n_M are $n_{I\!P} = 1.29 \pm 0.03(\text{stat})\pm0.07(\text{syst})$ and $n_M = 0.3 \pm 0.3(\text{stat})\pm0.6(\text{syst})$. The quoted systematic uncertainties include not only those described above associated with the treatment of the putative meson contribution, but also the experimental uncertainties associated with the measurement of $F_2^{D(3)}$, where the correlations between certain systematic uncertainties were taken into account.

Correcting for the integration over t by assuming peripheral t dependencies $\propto e^{b_{I\!P}t}$,$e^{b_M t}$ ($b_{I\!P} = 6$, $b_M = 5$) and linear trajectories of the form $\alpha_{I\!P,M}(t) = \alpha_{I\!P,M}(0) + \alpha'_{I\!P,M}\cdot t$ and assuming $\alpha'_M = 1$, $\alpha'_{I\!P} = 0.3$ yields values of $\alpha_{I\!P}(0) = 1.18 \pm 0.02(\text{stat})\pm0.04(\text{syst})$ and $\alpha_M(0) = 0.6\pm0.1(\text{stat})\pm0.3(\text{syst})$ for the intercepts of the pomeron and meson trajectories respectively. The value of α_M is entirely consistent with that expected for the trajectory associated with the $f_2^0(1270)$ meson. With these assumed values of $b_{I\!P}$ and b_M the value of $\alpha_{I\!P}(0)$ is somewhat larger than that obtained in some parameterisations of soft hadronic interactions [25, 26, 27, 28].

Although the data constrain modestly the intercept of any meson component, the overall normalisation is not well constrained in the presence of any interference between the pomeron and meson components. Figure 7 shows an example of a fit ($\chi^2/ndf = 170/156$) in which the relative phase angle is set to 45^o. In this parameterisation of the data the dominant contributions to the observed deviations from factorisation come from the interferences between the two components. The data do not require the presence of additional non–degenerate meson trajectories: a fit permitting a further non–interfering trajectory with intercept $\alpha_{M2}(0) = 0$ results in an equally good description of the data, in which the magnitude of this term is compatible with zero.

It is important to note that other explanations for the observed breaking of factorisation shown in figure 5 are possible. In a partonic interpretation of the diffractive exchange (see section 7), such an effect may occur if the β or $x_{I\!P}$ dependence differs for "valence" or "sea" components [29]. In models based on the exchange of two perturbative gluons the dependence of the diffractive cross section on $x_{I\!P}$ may be related to the x dependence of the gluon distribution in the proton $xG(x,k^2)$. Recent calculations of this type suggest that the scale k^2 at which the gluon distribution in the proton is sampled increases with β leading to a higher effective value of n at large β than at small β. One such calculation [33, 34] is compared to the data in figure 8. Given the large uncertainty in the gluon distribution in the proton at the scale relevant in this model ($\sim 1\,\mathrm{GeV}^2$), the level of agreement at $x_{I\!P} < 10^{-2}$ is noteworthy. Furthermore, it is intriguing to note that this calculation differs most from the data in precisely the region of low β and high $x_{I\!P}$ where the phenomenological analysis described above suggests that meson exchange may be important.

7 The Partonic Structure of Diffractive Exchange

In the factorisable prescription proposed in [23], $\int \mathrm{d}x_{I\!P} F_2^{D(3)}(\beta, Q^2, x_{I\!P})$ describes the partonic structure of the diffractive exchange in an analogous way to $F_2(x,Q^2)$ in the case of the proton. Despite the observation of non-factorisation of the measured cross-section, performing the integration over $x_{I\!P}$ provides a measurement of the average deep-inelastic structure of whatever colourless isospin-conserving exchanges contribute in the kinematic domain accessed. In the formalism of Trentadue and Veneziano [35], the integrated structure function is closely related to the fracture function for a semi-inclusive hadronic final state with a leading isospin-$\frac{1}{2}$ baryon. As such, it can be interpreted in the context of the QCD evolution of the parton densities of the leading Regge pole exchange coupling to the isospin-$\frac{1}{2}$ baryon.

We define

$$\tilde{F}_2^D(\beta, Q^2) = \int_{x_{I\!P}=0.0003}^{x_{I\!P}=0.05} F_2^{D(3)}(\beta, Q^2, x_{I\!P})\mathrm{d}x_{I\!P}$$

which is proportional to the structure function for the exchange averaged over the range, $t_{min}(x_{I\!P}) \geq t > -1\,\mathrm{GeV}^2$ and $0.0003 \leq x_{I\!P} \leq 0.05$. Where no measurement has been made in the $x_{I\!P}$ range of integration, the fit shown in figure 4 is used to extrapolate and the uncertainty arising from possible variations in the dependence on $x_{I\!P}$ included in the error calculation. Fig. 9 shows $\tilde{F}_2^D(\beta, Q^2)$ as a function of Q^2 for fixed β and as a function of β for fixed Q^2.

At fixed Q^2, $\tilde{F}_2^D(\beta, Q^2)$ displays little dependence on β. There is no evidence for the fall with increasing parton momentum fraction characteristic of the structure functions of hadrons.

$\tilde{F}_2^D$ shows no large variation with Q^2, though violations of scale invariance are clearly established. The most striking feature is that a rise with $\ln Q^2$ persists to values of β far in excess of the point ($x \sim 0.15$) at which the structure of the nucleon is dominated by valence quarks rather than by gluons, and $\frac{\partial F_2(x,Q^2)}{\partial \ln Q^2}$ correspondingly becomes negative [36]. The nature of the scaling violations of $\tilde{F}_2^D(\beta, Q^2)$ are thus in qualitative accord with the hypothesis of a substantial gluon component in the structure of the diffractive exchange.

Figure 10 shows a comparison between $\tilde{F}_2^D$ and the equivalent integral, $\tilde{F}_2^{I\!P}$, of the pomeron component extracted from the fit shown in figure 6 and described in section 6. The logQ^2 dependence of $\tilde{F}_2^{I\!P}$ follows closely that of $\tilde{F}_2^D$, with it's rise with increasing Q^2 persisting to large β. In such a parameterisation, $\tilde{F}_2^{I\!P}$ is proportional to the structure function of the pomeron $F_2^{I\!P}(\beta, Q^2)$. The conclusions of gluon dominance in the diffractive exchange which are drawn from the observed scaling violations of $\tilde{F}_2^D$ are therefore unaffected by the possible presence of sub–leading trajectories. An evaluation of $\tilde{F}_2^D$ using only those data in the kinematic range $x_{I\!P} < 10^{-2}$ is compatible with $\tilde{F}_2^{I\!P}$, displaying the same characteristic violations of scaling with logQ^2.

A QCD analysis of $\tilde{F}_2^D(\beta, Q^2)$ confirms this qualitative picture [6, 7]. A $u + d + s$ flavour singlet quark and a gluon distribution are parameterised at a starting scale, $Q_0^2 = 2.5$ GeV^2, as

$$x_{_{i/I\!P}} \cdot f_i(x_{_{i/I\!P}}) = A_i \; x_{_{i/I\!P}}^{B_i} \; (1 - x_{_{i/I\!P}})^{C_i}$$

where $i = q, g$ and $x_{_{i/I\!P}}$ is the fraction of the exchange momentum carried by the parton. These parton distributions are then evolved using DGLAP [17] evolution to $Q^2 > Q_0^2$, with the values of $A_{q,g}$, $B_{q,g}$ and $C_{q,g}$ as fit parameters. Since additional theoretical input is required to normalise the structure function, no momentum sum rule is imposed [3].

Charm quarks are not explicitly introduced into the parton distributions, but are included through boson-gluon fusion using the procedure followed in [15, 37].

Figure 11a shows the best fit obtained for $\tilde{F}_2^D$ when A_g is constrained to be zero, and only quarks contribute at the starting scale. Because of the persistence of rising $\ln Q^2$ scaling violations to high values of β, no such parameterisation is acceptable (confidence level CL = 0.00013%). An excellent (CL = 47.8%) fit, shown in figure 11b, can be obtained when gluons are also introduced at the starting scale. An otherwise identical QCD analysis of $\tilde{F}_2^{I\!P}$ leads to the same conclusions. There is no theoretical consensus that the DGLAP evolution equations are appropriate for the calculation of the evolution of the parton densities with Q^2 at the highest values of β ($\beta > 0.7$). Excluding the data at $\beta = 0.9$ from the QCD analysis does not affect the conclusions drawn in any way.

The parton densities in the mixed quark and gluon fit at $Q^2 = 5$ GeV^2 and $Q^2 = 65$ GeV^2 are shown in figure 12, along with the integrated momentum fractions carried by quarks and gluons as a function of Q^2. At $Q^2 = 5$ GeV^2, a "leading" gluon behaviour is observed, in which the exchange is dominated by gluons carrying fractional momentum, $x_{g/I\!P} > 0.9$, tending to a singularity as $x_{g/I\!P} \to 1$. As Q^2 increases, the gluon distribution is evolved by the DGLAP equations to lower values of β. Throughout the Q^2 range, in excess of 80% of the momentum is carried by gluons, with a decrease in this fraction as Q^2 increases. These conclusions are supported by H1 analyses of the hadronic final state in deep-inelastic diffractive events [8, 38, 39, 40]. The "leading" gluon behaviour is expected in the model of deep–inelastic diffraction proposed by Buchmüller and Hebecker and others [41].

[3] In any case, it is far from clear that a momentum sum rule should exist for space-like exchanges [35].

8 Summary and Conclusions

Diffractive deep-inelastic ep scattering at HERA has been investigated using the data taken in 1994 with the H1 detector. At the present level of experimental precision, the dependence on $x_{I\!P}$ of the diffractive structure function $F_2^{D(3)}(\beta, Q^2, x_{I\!P})$ is found to vary with β but not with Q^2. The factorisation from the cross section for diffractive deep–inelastic scattering of a universal term describing a diffractive flux associated with the proton is therefore shown to be untenable. The observed deviations from factorisation are shown to be consistent with a contribution to $F_2^{D(3)}$ from meson exchange. The leading pomeron exchange trajectory is found to have an intercept which is slightly higher that obtained in some parameterisation of soft hadronic physics. The unambiguous observation of scaling violations in the Q^2 dependence of $\tilde{F}_2^D(\beta, Q^2)$ for fixed β in the form of a rising $\log Q^2$ dependence for $\beta \lesssim 0.65$ is interpreted in the framework of QCD in terms of a substantial contribution of gluons to the sub–structure of diffractive exchange. A DGLAP motivated QCD fit is found to require that roughly 80% of the momentum transfer in diffractive exchange be attributed to gluon exchange at $Q^2 \simeq 5$ GeV^2 and further that the diffractive exchange evolves as if dominated by a leading gluon.

Acknowledgements

We are grateful to the HERA machine group whose outstanding efforts have made and continue to make this experiment possible. We thank the engineers and technicians for their work in constructing and now maintaining the H1 detector, our funding agencies for financial support, the DESY technical staff for continual assistance, and the DESY directorate for the hospitality which they extend to the non–DESY members of the collaboration. We also acknowledge much help with the theoretical interpretation of our results from many colleagues. In particular we thank Z. Kunszt for enlightening discussions, and for providing the facilities to verify the results of our QCD analysis.

References

[1] ZEUS Collaboration, M.Derrick et al., Phys. Lett. **B315** (1993) 481.

[2] H1 Collaboration, T. Ahmed et al., Nucl. Phys. **B429** (1994) 477.

[3] H1 Collaboration, T. Ahmed et al., Phys. Lett. **B348** (1995) 681.

[4] ZEUS Collaboration, M.Derrick et al., Z. Phys **C68** (1995) 569.

[5] A. Mehta, "Comparison of Diffractive and Non–Diffractive Deep–Inelastic Scattering", in proceedings of Photon '95, Workshop on photon–photon interactions, 8-13 April 1995, Sheffield, England, p. 313.

[6] J. P. Phillips, "Rapidity Gap Events at HERA and the Structure of the Pomeron", in Proc. of the International Workshop on Deep–Inelastic Scattering and Related Topics, Paris, France, April 1995, p.359.

[7] J. B. Dainton, "Deep–Inelastic Physics with H1 at the HERA ep Collider", in Proc. of the International Workshop on Deep–Inelastic Scattering and Related Topics, Paris, France, April 1995, p.37;
J. B. Dainton, "Deep–Inelastic Electron-Proton Diffraction", DESY **95-228**.

[8] A. Mehta, "Deep–Inelastic Diffraction", proceedings of Topical Conference on Hard Diffractive Processes, February 18-23 1996, Eilat, Israel.

[9] H1 Collaboration, I. Abt et al., , "The H1 Detector at HERA", DESY preprint 93–103 (July 1993); *idem* DESY internal report H1–96–01 (March 1996).

[10] H1 Collaboration, "Leading Neutron Production in Deep-Inelastic ep Scattering at HERA", pa02-63, contribution to 28th International Conference on High Energy Physics 25 - 31 July 1996, Warsaw, Poland.

[11] B. List, "Diffraktive $J/\psi-$Produktion in Elektron–Proton–Stößen am Speicherring HERA", Diploma Thesis (Tech. Univ. Berlin), 1993 (unpublished).

[12] R. Engel, Proceedings of the XXIXth Rencontre de Moriond (1994) 321.

[13] T. Sjöstrand, Comp. Phys. Comm. 39 (1986) 347;
T. Sjöstrand and M. Bengtsson, Comp. Phys. Comm. 43 (1987) 367;
T. Sjöstrand and M. Bengtsson, Comp. Phys. Comm. 46 (1987) 43.

[14] U. Bassler and G. Bernardi Nucl. Instr. and Meth.**A361** (1995) 118.

[15] H1 Collaboration, T. Ahmed et al., , "A Measurement and QCD Analysis of the Proton Structure Function $F_2(x, Q^2)$ at HERA", Nucl. Phys. **B470** (1996) 3.

[16] H. Jung Comp. Phys. Comm. **67** (1992) 465.

[17] Yu. L. Dokshitzer, JETP **46** (1977) 641.
V. N. Gribov and L. N. Lipatov, Sov. Journ. Nucl. Phys. **15** (1972) 78.
G. Altarelli and G. Parisi, Nucl. Phys. **B126** 1977 298.

[18] L. Lönnblad, Computer Phys. Comm. **71** (1992) 15.

[19] G. Ingelman, Proceedings of the Workshop on Physics at HERA, vol. 3, eds. W. Buchmüller, G. Ingelman, DESY (1992) p.1366.

[20] A. Kwiatkowski, H. Spiesberger and H.-J. Möhring, Computer Phys. Comm. **69** (1992) 155.

[21] H1 Collaboration, T. Ahmed et al., , Nucl.Phys. **B468** (1996)3

[22] G. A. Schuler and H. Spiesberger, Proceedings of the Workshop on Physics at Hera, vol. 3, eds. W. Buchmüller, G. Ingelman, DESY (1992) p.1419.

[23] G. Ingelman and P. Schlein, Phys. Lett. **B152** (1985) 256.

[24] See for example P.Collins, "An Introduction to Regge Theory & High Energy Physics ", Cambridge University Press, Cambridge (1977).

[25] H. Cheng, J. K. Walker and T. T. Wu, Phys. Rev. Lett. **B44** (1973) 97.

[26] H. Cheng, and T. T. Wu, Phys. Rev. Lett. **22** (1969) 666, Phys. Rev. **182** (1969) 1852, 1868, 1873, 1899.

[27] C. Bourrely, J. Soffer and T. T. Wu, Phys. Rev. **D19** (1979) 3249.

[28] A. Donnachie and P. Landshoff, Nucl. Phys. **B303** (1988) 634.

[29] N. Nikolaev and B. Zakharov, Z. Phys. **C53** (1992) 331.

[30] E. Barberis, Workshop on Deep–Inelastic Scattering and QCD, Rome, 1996.

[31] ZEUS Collaboration, M.Derrick et al., accepted by Z. Phys **C**, DESY 96-018.

[32] M. Gluck, E. Reya, A. Vogt, Z.Phys. **C53** (1992) 651-656.

[33] M. Wüsthoff, "Photon Diffractive Dissociation in Deep Inelastic Scattering", DESY 95-166.

[34] J. Bartels, H. Lotter, M. Wusthoff, DESY-96-026.

[35] L. Trentadue and G. Veneziano, Phys. Lett. **B323** (1994) 201.

[36] NMC Collaboration, M. Arneodo et al., Phys. Lett. **B364** (1995) 107;
BCDMS Collaboration, A. C. Benevuti et al., Phys. Lett. **B223** (1989) 485.

[37] C. Pascaud, F. Zomer, LAL preprint LAL/94-42.

[38] H1 Collaboration, " Measurements of Jet Production and Energy Flow in Diffractive *ep* Interactions at HERA", pa02-62, contribution to 28th International Conference on High Energy Physics 25-31 July 1996. Warsaw, Poland.

[39] H1 Collaboration, " Thrust Jet Analysis of Deep–Inelastic Large Rapidity Gap Events at HERA", pa02-68, contribution to 28th International Conference on High Energy Physics 25-31 July 1996. Warsaw, Poland.

[40] H1 Collaboration, " A Measurement of the Production of $D^{*\pm}$ Mesons in Deep–Inelastic Diffractive Interactions at HERA", pa02-60, contribution to 28th International Conference on High Energy Physics 25-31 July 1996. Warsaw, Poland.

[41] W. Buchmüller and A. Hebecker, Phys. Lett. **B 355** (1995) 573.

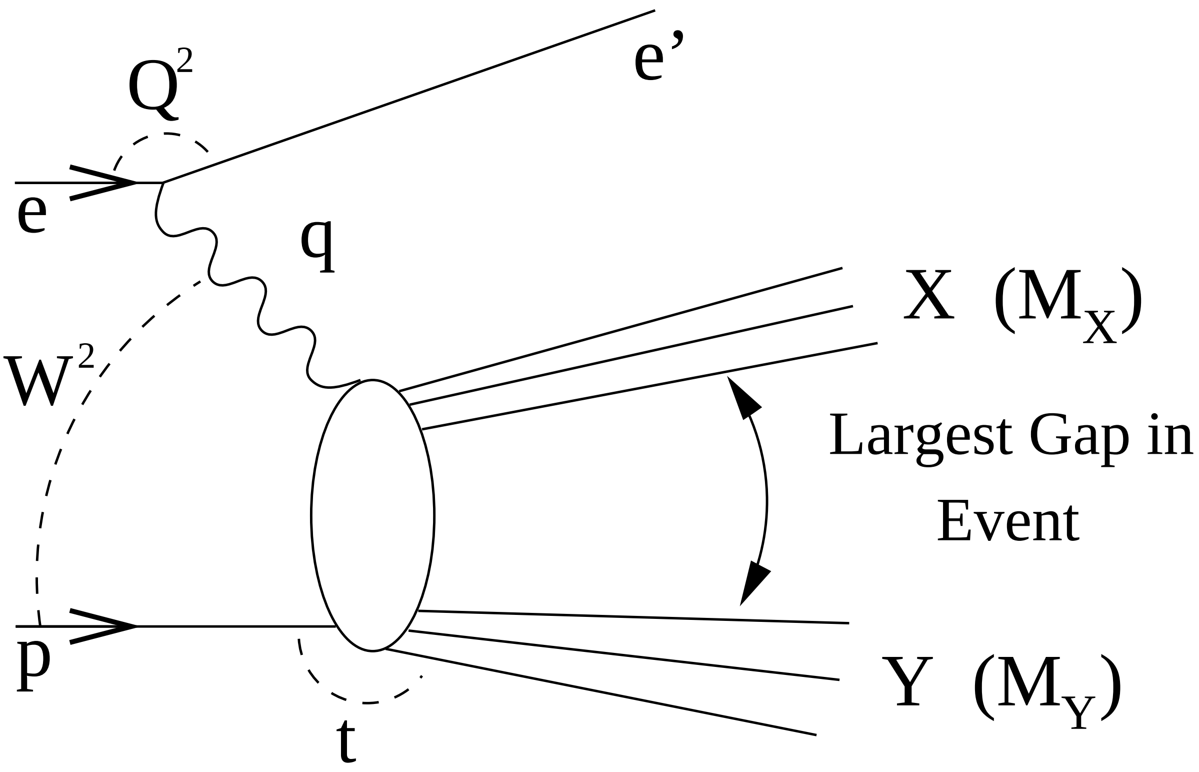

Figure 1: Schematic illustration of the method of selecting events to define a diffractive cross-section, showing the definitions of the kinematic variables discussed in the text.

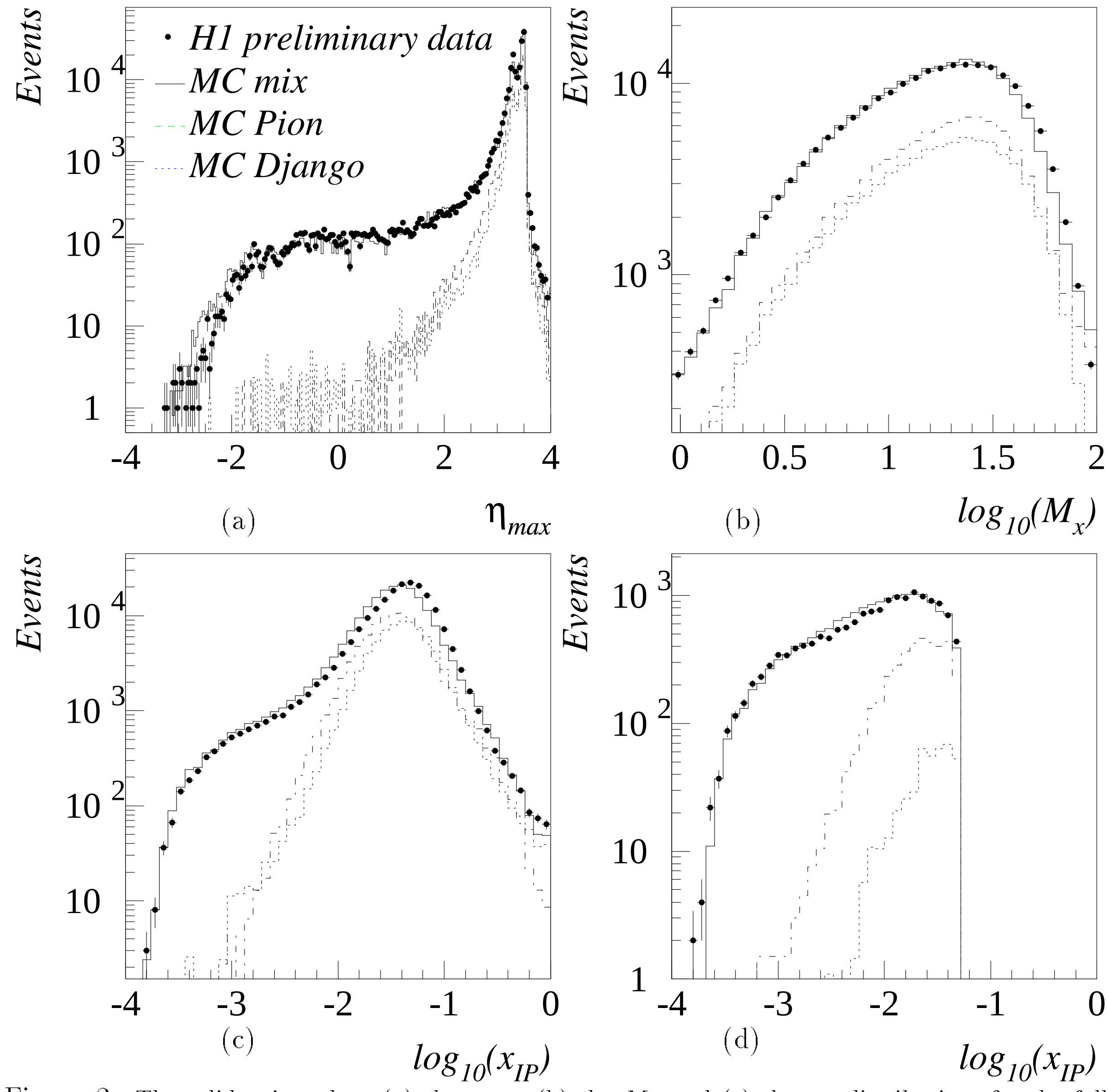

Figure 2: The solid points show (a) the η_{max}, (b) the M_X and (c) the $x_{I\!P}$ distributions for the full DIS sample without a diffractive selection and (d) $x_{I\!P}$ distribution for the diffractive DIS sample. All distributions have not been corrected for detector effects. Also shown as the solid histogram is the prediction of the Monte Carlo mixture (RAPGAP $I\!P$, RAPGAP π, DIFFVM, DJANGO), dashed histogram is expectation from RAPGAP π and dotted that from DJANGO.

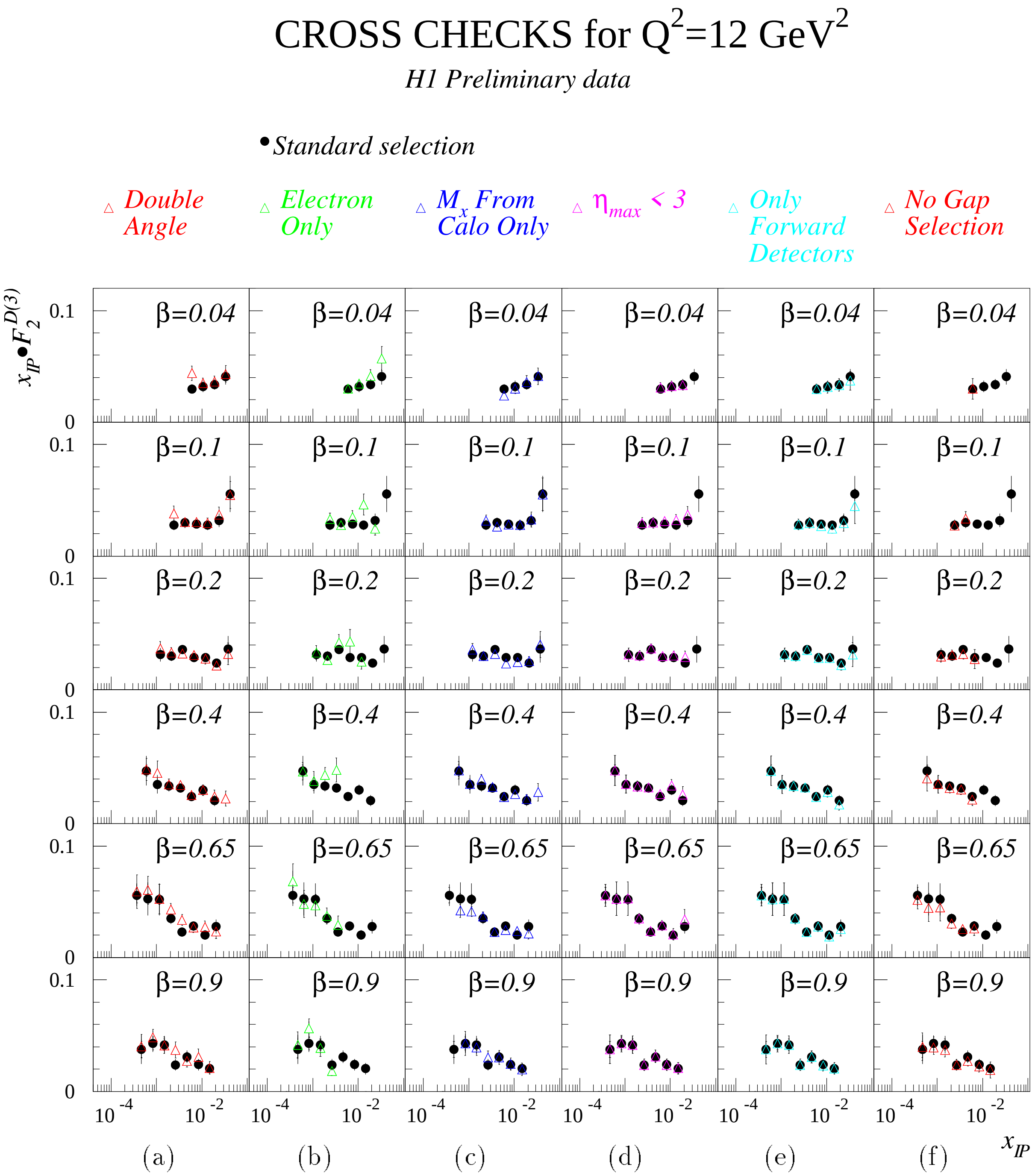

Figure 3: Effect of changing kinematic reconstruction techniques and diffractive selection on the measured $F_2^{D(3)}$ for $Q^2 = 12\,\mathrm{GeV}^2$. This values of Q^2 is chosen as here the statistical precision of the data is greatest, such that any small systematic trends may be observed. The solid circles show the data measured using the standard analysis. In each of the six columns, these data are compared to those obtained with a modified analysis technique in which (a) x and Q^2 were reconstructed with the double angle method, (b) x and Q^2 were reconstructed from the scattered positron alone, (c) the mass M_X was reconstructed from the calorimeter alone, (d) an η_{max} cut of 3 was used, (e) only the forward detectors were used, (f) no rapidity gap selection at all was used.

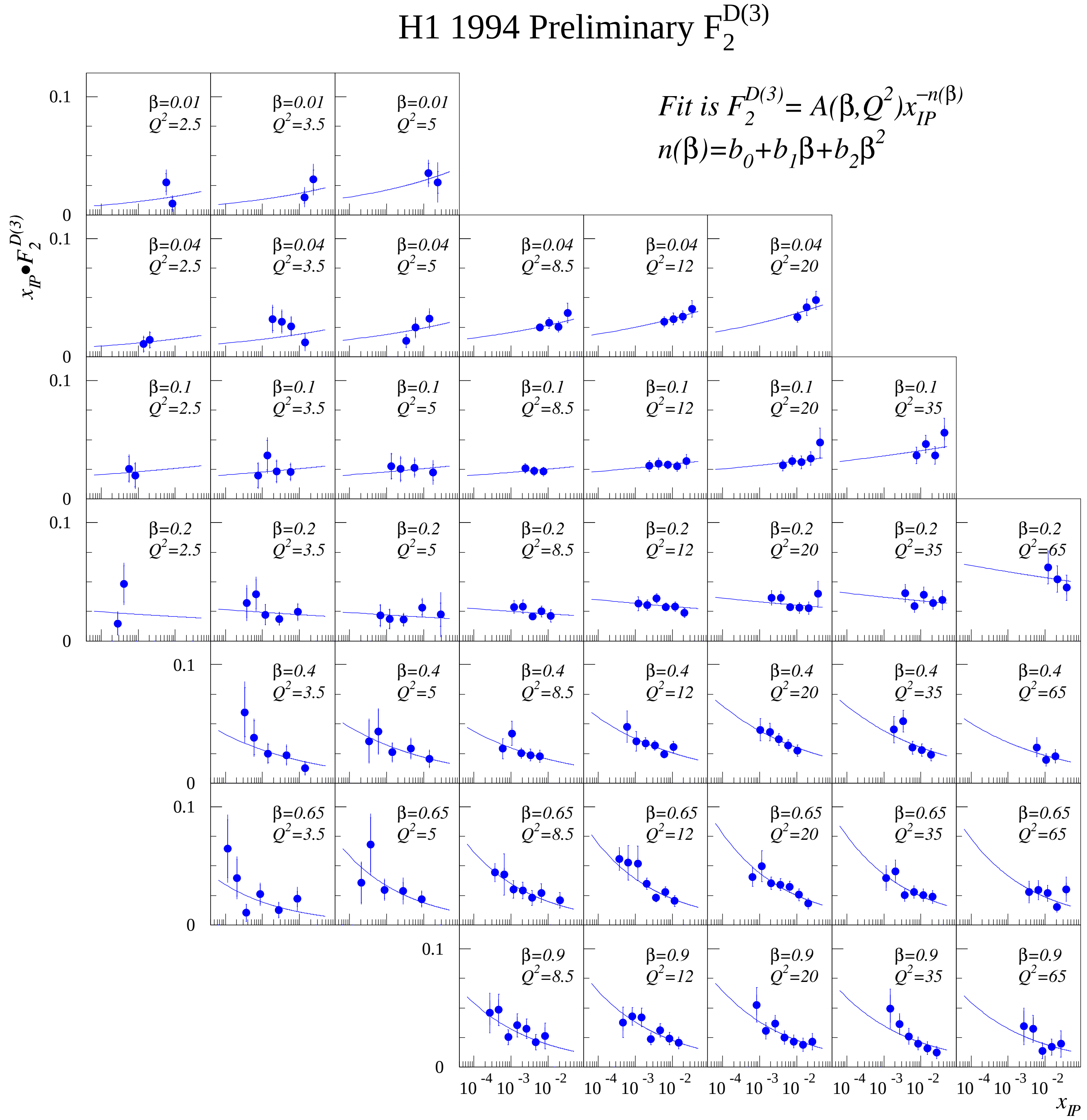

Figure 4: Results for the value of n when $F_2^D(\beta, Q^2, x_{I\!P})$ is fitted to the form, $\left(\frac{1}{x_{I\!P}}\right)^{n(\beta)}$. Statistical and systematic errors are added in quadrature. The curves are from the overall parametrisation of the $x_{I\!P}$ dependence of $F_2^{D(3)}$ shown in fig. 4 and described in the text.

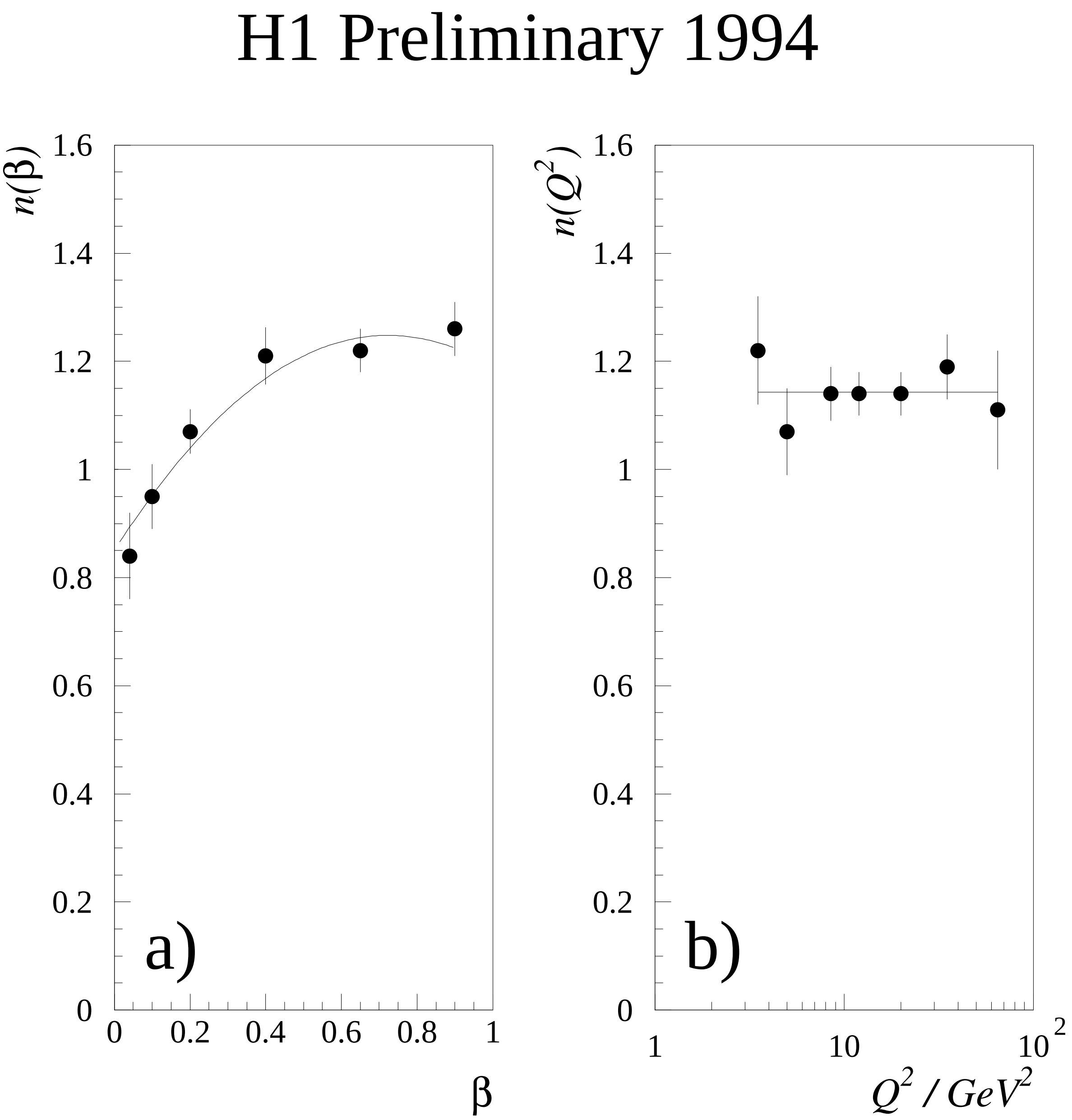

Figure 5: $x_{I\!P} \cdot F_2^{D(3)}(\beta, Q^2, x_{I\!P})$ together with a fit of the form $F_2^{D(3)} = A(\beta, Q^2)/x_{I\!P}{}^{n(\beta)}$. The experimental errors are statistical and systematic added in quadrature.

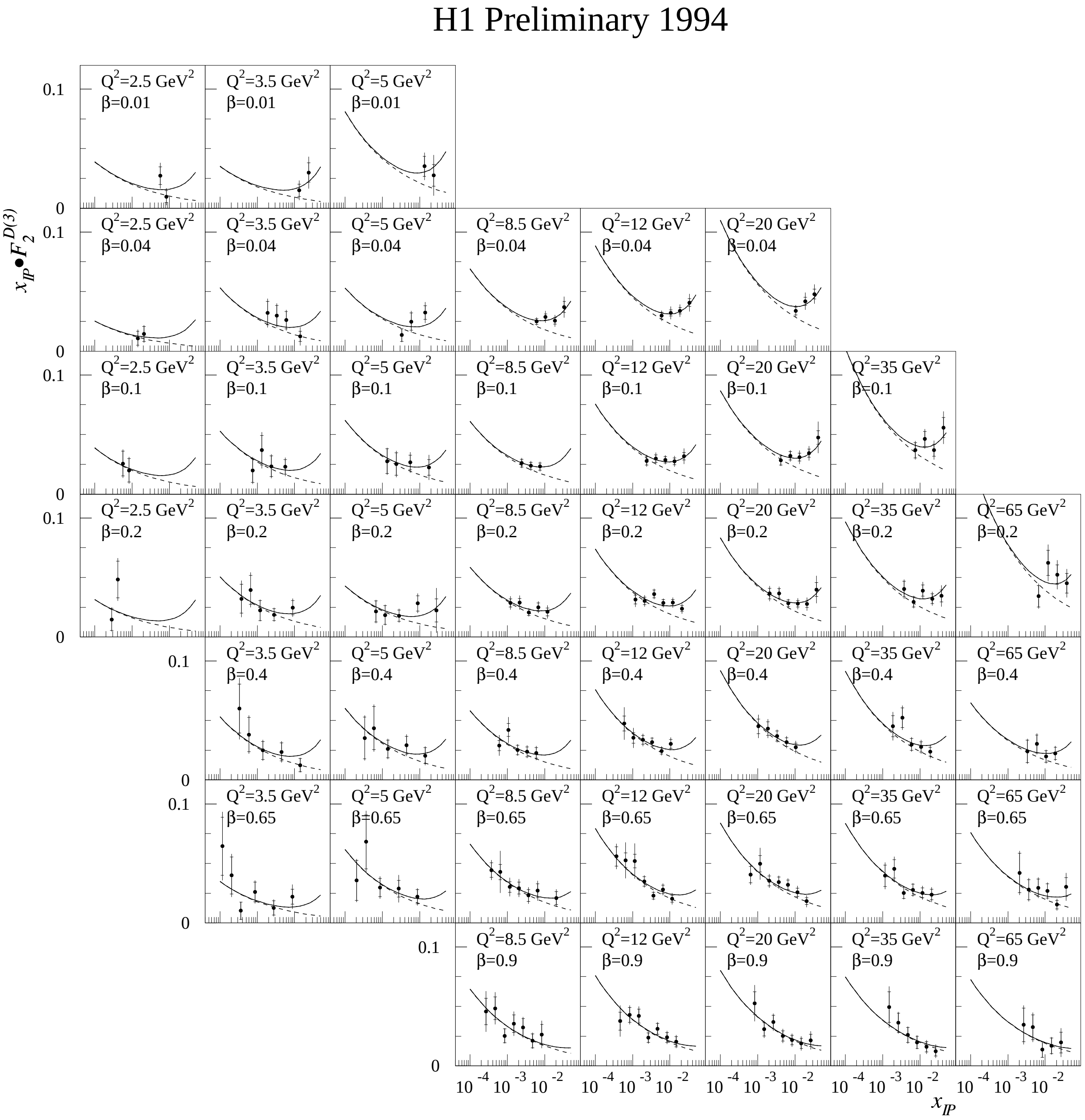

Figure 6: $x_{I\!P} \cdot F_2^{D(3)}(\beta, Q^2, x_{I\!P})$ together with a fit in which a pomeron component with trajectory $\alpha_{I\!P}(t)$ contributes together with a meson component with trajectory $\alpha_M(t)$. The pomeron and meson components do not interfere (see text for details of the fit). The dashed line shows the contribution from the pomeron component; the solid line show the total contribution from the sum of the pomeron and meson components. The experimental errors are statistical and systematic added in quadrature.

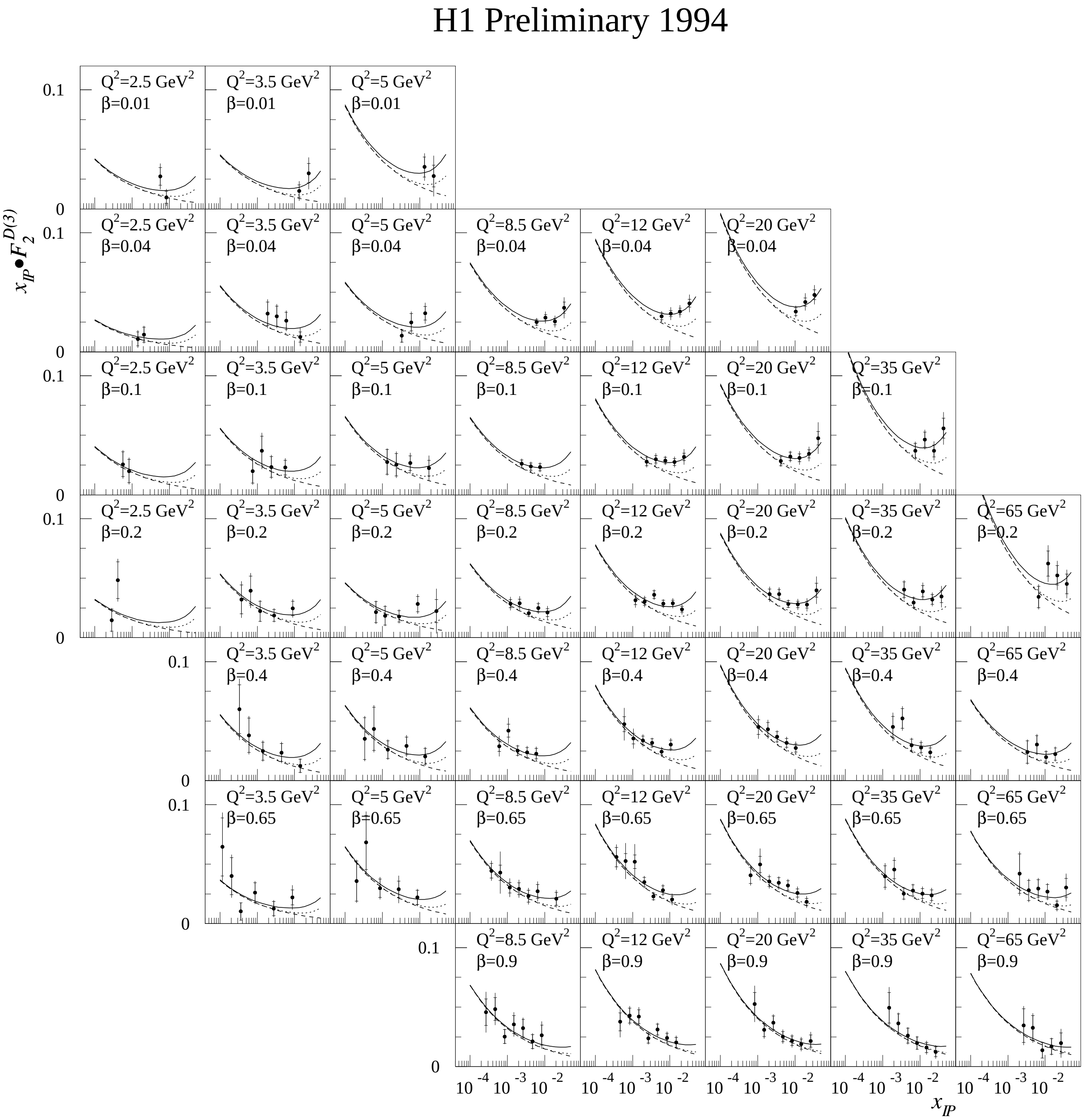

Figure 7: $x_{I\!P} \cdot F_2^{D(3)}(\beta, Q^2, x_{I\!P})$ together with a fit in which a pomeron component with trajectory $\alpha_{I\!P}(t)$ contributes together with a meson component with trajectory $\alpha_M(t)$ where the pomeron and meson components interfere with a relative phase of 45^o. The dashed line shows the contribution from the pure pomeron intensity; the dotted line shows the sum of the pure pomeron and meson intensities, the solid line show the total contribution. The experimental errors are statistical and systematic added in quadrature.

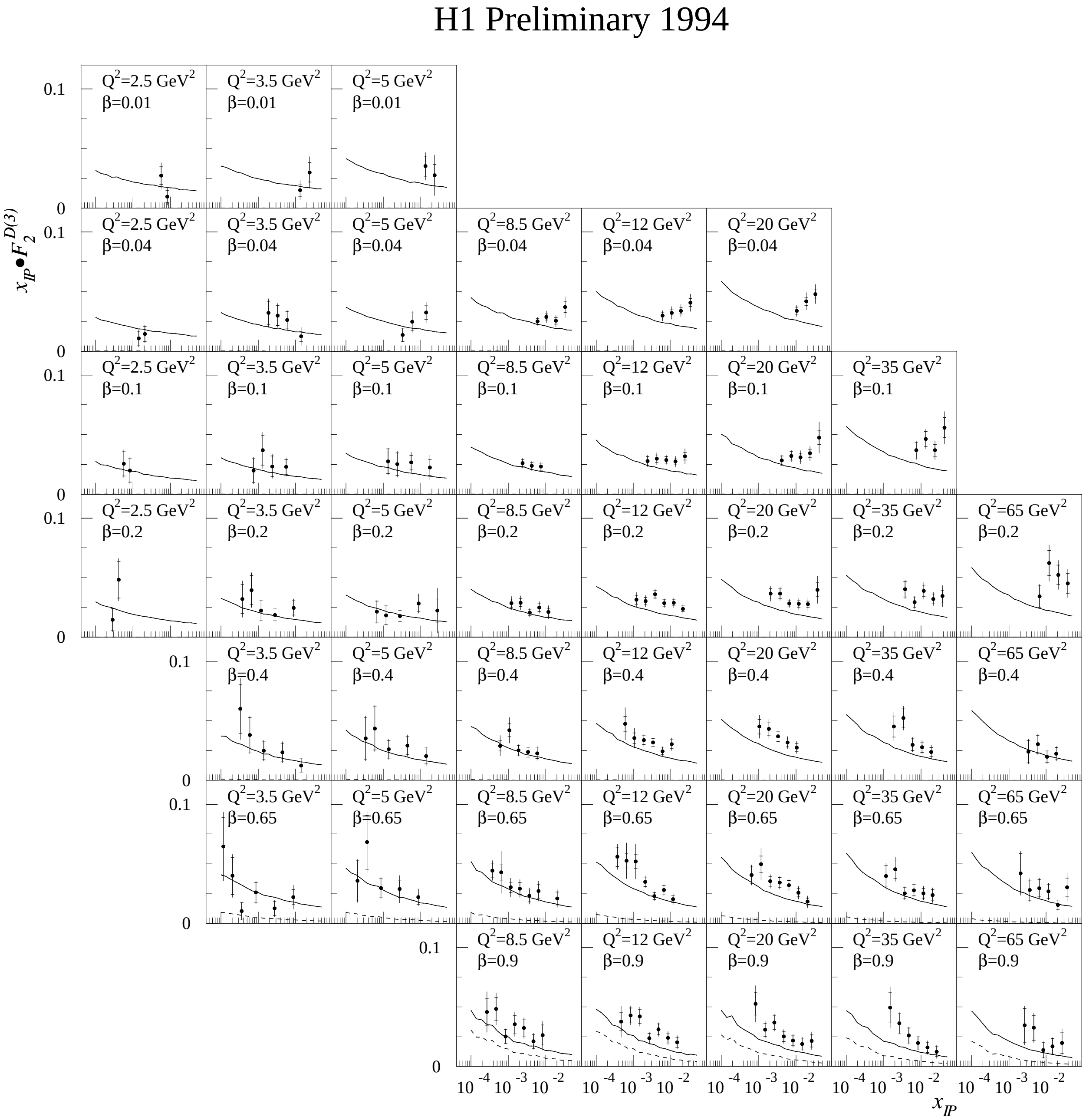

Figure 8: $x_{I\!P} \cdot F_2^{D(3)}(\beta, Q^2, x_{I\!P})$ compared with the calculation of Wüsthoff (see text). The dashed curve is the contribution to $F_2^{D(3)}$ from longitudinally polarised photons, the solid line is the total. The error arising from the determination of the gluon distribution in the proton is not shown. The experimental errors are statistical and systematic added in quadrature.

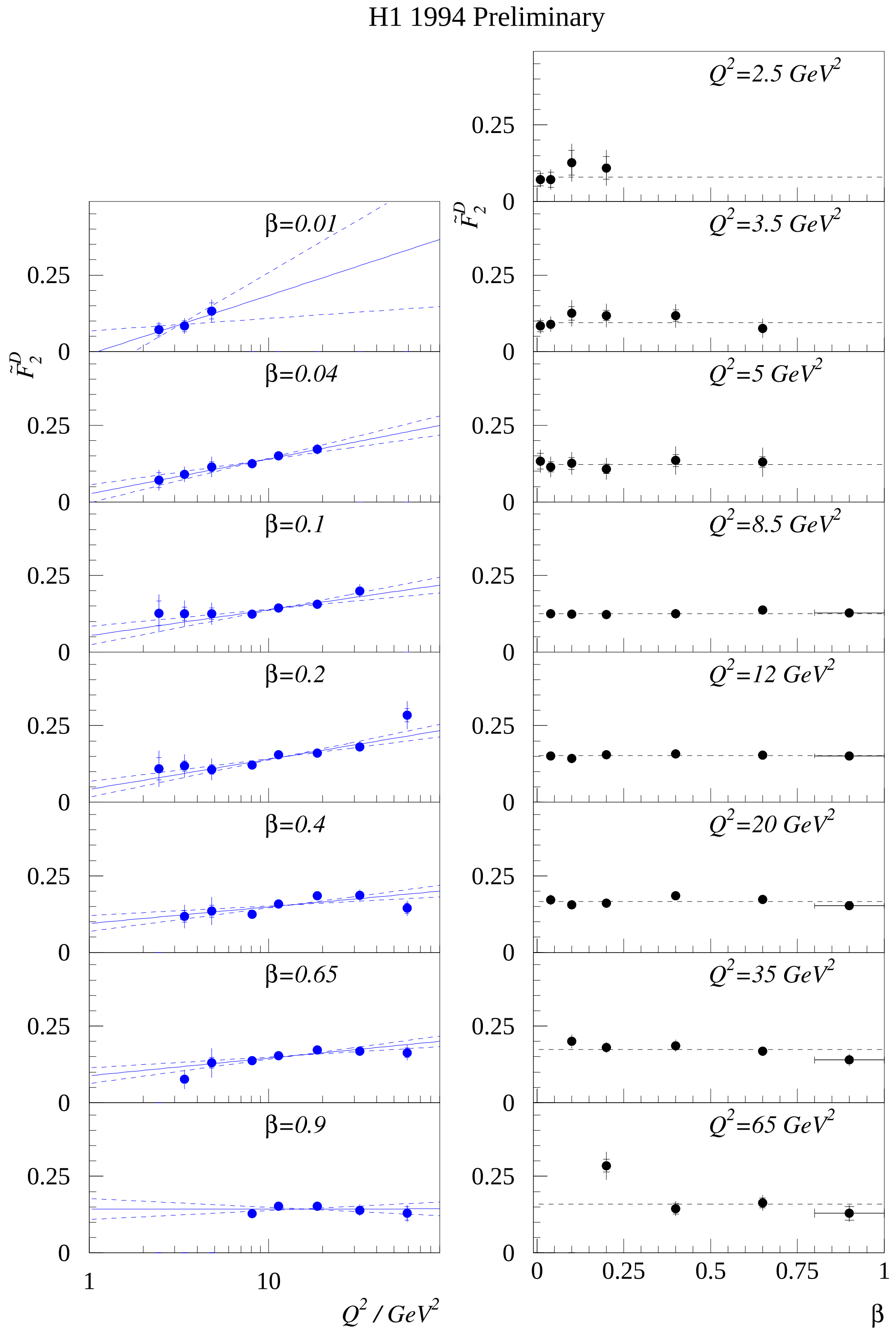

Figure 9: $\tilde{F}_2^D(\beta, Q^2)$ as a function of Q^2 for different β values (left) and as a function of β for different Q^2 values (right); the superimposed lines correspond to the best fit to a linear dependence on $\ln Q^2$ (continuous) and $\pm 1\sigma$ (dashed) in the Q^2 dependences, and to a constant dependence in the β dependences (dashed).

H1 Preliminary 1994

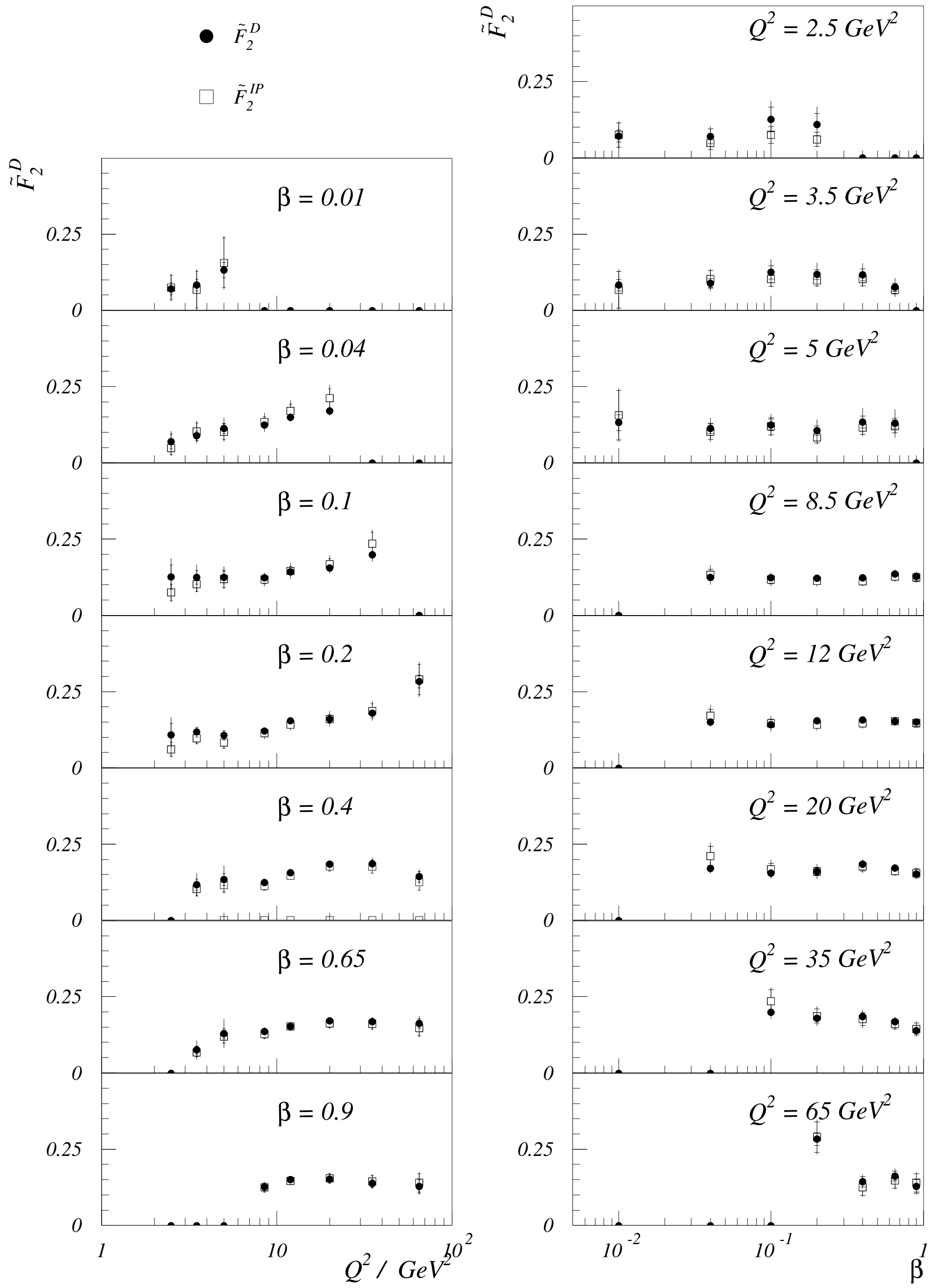

Figure 10: Comparison of $\tilde{F}_2^{IP}(\beta, Q^2)$ and $\tilde{F}_2^D(\beta, Q^2)$ as a function of Q^2 for different β values (left) and as a function of β for different Q^2 values (right).

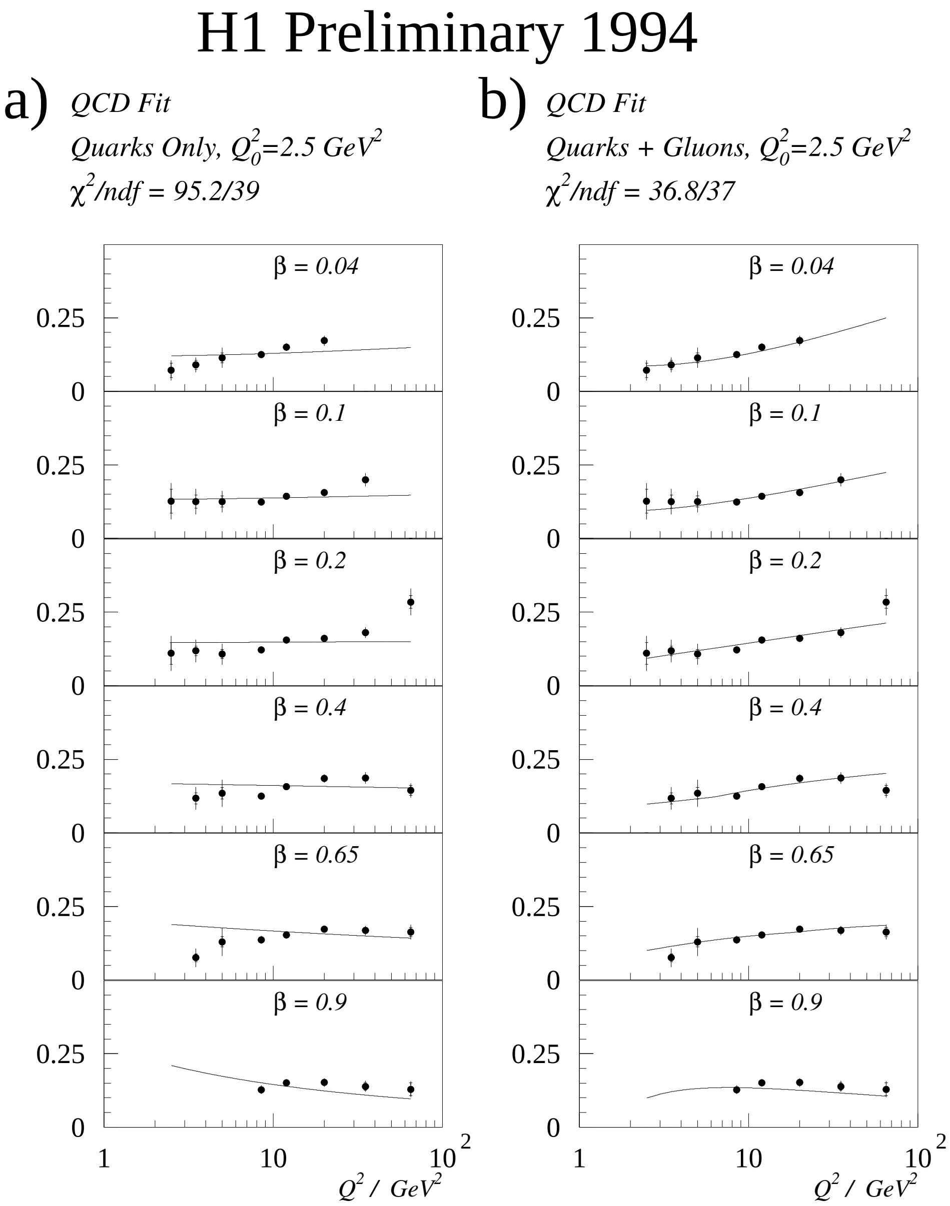

Figure 11: a) DGLAP QCD comparison of the (β, Q^2) dependence of $\tilde{F}_2^D$ assuming only quarks at the starting scale of $Q_0^2 = 2.5$ GeV^2; the DGLAP equations evolve in Q^2 and fail to reproduce the tendency in the data for linearly rising scaling violations at larger β; b) DGLAP QCD comparison of the (β, Q^2) dependence of $\tilde{F}_2^D$ assuming both quarks and gluons at the starting scale of $Q_0^2 = 2.5$ GeV^2, showing the agreement with linearly rising scaling violations at larger β.

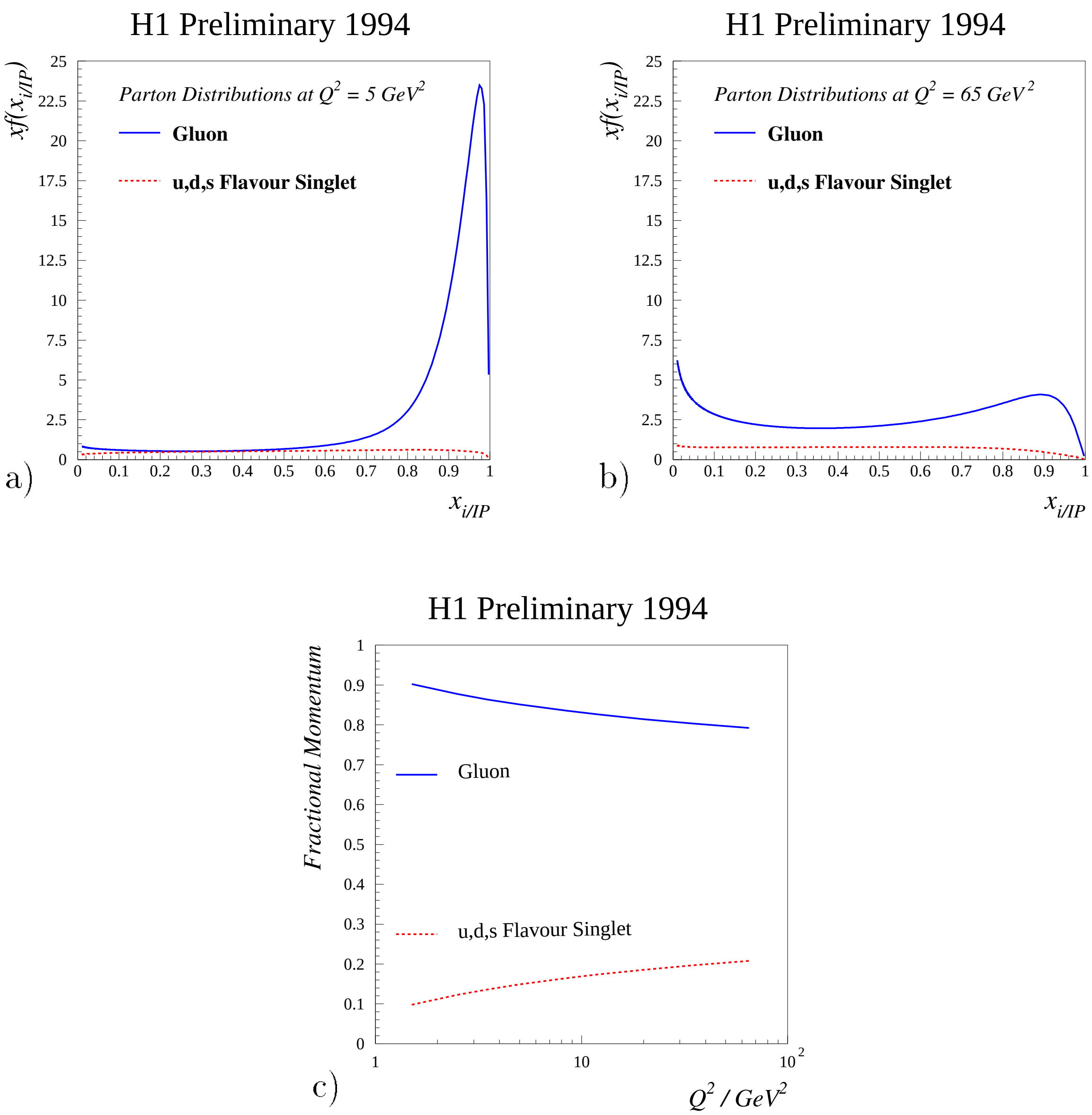

Figure 12: Quark and gluon momentum weighted distributions in fractional momenta $x_{g/I\!P}$ and $x_{q/I\!P}$ for diffractive exchange averaged over $x_{I\!P}$ and t extracted using the DGLAP QCD fit at a) $Q^2 = 5\,\mathrm{GeV}^2$ and b) $Q^2 = 65\,\mathrm{GeV}^2$; c) fraction of the total momentum carried by quarks and by gluons as a fraction of the total momentum transfer in diffractive exchange as a function of Q^2. No errors are shown because of ambiguity in their determination due to the tendency of the solution to peak at large $x_{g/I\!P}$.